Thermal forcing modulates North American Monsoon intensity

M. Lofverstrom[1*] and K. Thirumalai[1]

[1*]Department of Geosciences, University of Arizona, 1040 E. 4th Street, Tucson, 85721, AZ, USA.

*Corresponding author(s). E-mail(s): lofverstrom@arizona.edu; Contributing authors: kaustubh@arizona.edu;

1 Matters Arising

Understanding the response of monsoon dynamics to climatic forcing is cru-cial for anticipating future shifts in freshwater availability across the global tropics. In this regard, a recent study [1] concludes that precipitation within the core of the North American Monsoon (NAM) should be understood as "*convectively enhanced orographic rainfall in a mechanically forced stationary wave, not as a classic, thermally forced tropical monsoon.*" Using model simu-lations under altered surface conditions, this study suggests that interactions of the extratropical jet stream with Mexico's Sierra Madre Occidental (SMO) orography are a first-order control on the NAM under past and future global change. While we agree that the presence of orography enhances rainfall out-side land-sea thermal gradients alone [2], we believe that their experiments and analysis are not adequately designed to refute the central importance of thermally-direct forcing in modulating past and future NAM rainfall.

Mechanically forced stationary waves — planetary waves more broadly — owe their existence to conservation of potential vorticity following the fluid motion [3, 4]. In essence, horizontal winds induced by large-scale pressure anomalies are balanced by latitudinal variations of the Coriolis parameter; note that stationary waves cannot be maintained in an easterly mean flow that is conserving potential vorticity [3]. Thus, orographically-induced stationary waves (neglecting diabatic effects and boundary-layer interactions) manifest flows in quasi-geostrophic balance. Whereas the quasi-geostrophic approxi-mation (geostrophic wind $\gg$ ageostrophic wind) is valid over much of the

North Pacific domain, the approximation breaks down over the broader NAM region where the ageostropic wind component grows comparable to or even exceeds the strength of the geostrophic wind (Fig. 1a,b). This region of strong ageostrophic wind includes both oceanic and terrestrial portions of the NAM domain, suggesting that this breakdown of quasi-geostrophy is not primarily due to local boundary-layer interactions over the SMO topography. Note that their simulation with flattened SMO mountains (*FlatMex*) does not feature a similar dominance of ageostrophic flow in the broader NAM region (Fig. 1c), further emphasizing the importance of local topography for organizing convection that drives convergent (ageostrophic) flow in the lower troposphere.

The low-level wind is largely orthogonal to surface isobars along the western seaboard, flowing towards the low sea-level pressure over the Gulf of California and into western Mexico. This general feature is also present north of ∼27°N the *FlatMex* simulation (cf. Fig. 1d-f), supporting the inference that these onshore winds are sensitive to thermodynamic forcing [5], as opposed to local orographic effects. Additionally, the original article ignores the importance of thermodynamic forcing on Gulf of California moisture surges — a process known to influence NAM precipitation [6].

The authors further suggest that the mechanically forced stationary wave is excited when *"Mexico's Sierra Madre mountains deflect the extratropical jet stream towards the Equator"*. However, their analyses does not demonstrate an explicit dynamical link between core NAM intensity and the extratropical jet stream, which peaks during boreal winter and is more poleward and muted during summer. As shown in Fig. 1, the extratropical jet stream makes landfall around 50°N along the North American west coast, thousands of kilometers northwest of the core NAM region. The horizontal wind field proximal to the NAM region (Fig. 1; see also their Fig. 1 and Extended Data Fig. 3) is a thermally controlled and typically dry low-level jet in the marine boundary layer [7]. This feature is largely parallel to the western coastal orography, veering away from the coast at subtropical latitudes (Fig. 1), and is dynamically distinct from the extratropical jet stream [8]. Therefore, delineating a relationship between extratropical jet stream strength and NAM intensity necessitates a dynamical framework involving this low-level jet, which is not borne out by their analysis.

We argue that the experiments in the original paper have not been appropriately designed to disentangle the relative influences of thermally-direct circulation versus mechanically forced stationary waves (by the extratropical jet stream) on NAM intensity. For instance, their stationary wave model simulates westerly low-level winds impinging on the SMO orography in response to an easterly flow from their *FlatMex* experiment (Fig. 1c; see also their Methods and Fig. 2). The null hypothesis that this anomalous response arises due to SMO interactions with the extratropical jet stream has therefore not been adequately identified. We further note that their *FlatMex* and *FlatMexLowAlb* experiments do not refute diabtic heating as a primary control on the large-scale circulation in the NAM region — particularly given the importance of

ageostrophy north of ∼27ºN in the *FlatMex* simulation (Fig. 1c,f). Alternatively, we suggest that a combination of simulations wherein albedo is altered holding observed topography intact (the authors' experiments highlight the importance of local topography for organizing the NAM) and another where the SMO height is altered (e.g., ±50%) may help isolate thermal versus mechanical forcing of NAM rainfall. Arguably, such experiments will also be more relevant for NAM changes under geologically-recent paleoclimates as well as under future greenhouse forcing.

The premise that the NAM is primarily driven by mechanical wave forcing can be examined using past climates. If the authors' assertion is robust, the NAM should be reduced in a climate with a poleward-shifted extratropical jet stream (*i.e.*, weaker mechanical wave forcing at low latitudes) and a stronger thermal forcing. The mid-Holocene (∼6000 years before present) emerges as an ideal period for this comparison as Earth's topography was virtually identical to today, but thermal forcing was higher due to a precession-driven increase in boreal summer insolation. Fig. 2 shows a multi-model comparison of the simulated mid-Holocene climate compared to the pre-industrial reference period. This analysis reveals that the extratropical jet stream migrates poleward under mid-Holocene boundary conditions. Yet, in spite of *weaker* mechanical stationary wave forcing in the lower latitudes, the NAM is substantially *stronger* compared to the pre-industrial reference period — a result that is robustly shown across numerous mid-Holocene simulations [9, 10]. Hydroclimate-sensitive proxy data (see Ref. [11] and references therein) corroborate this result (Fig. 2c), and thereby additionally support the classic picture of a thermally-driven intensification of the mid-Holocene NAM. Furthermore, paleoclimatic investigations of intervals featuring pronounced global changes, such as the Last Glacial Maximum (∼21,000 years before present) and the Pliocene (5.3-3 million years before present) further establish the importance of thermal gradients in modulating NAM variability — be it via atmospherically-mediated meridional temperature contrasts over the North American continent [12] or via coastal land-sea temperature gradients [13].

Last, Extended Data Fig. 1 shows diurnal variations of 925 hPa winds and precipitation averaged from 3-hourly data from the ERA5 reanalysis product [14]. The diurnal cycle exhibits the quintessential fingerprints of a thermally driven monsoon: an onshore flow in the mid- to late afternoon that coincides with strong convection and precipitation, and a reversal of the flow during the night and morning hours when convection is suppressed. This also helps explain the increased core monsoon precipitation under strengthened boreal summer insolation during the mid-Holocene (Fig. 2). Moreover, the diurnally reversing onshore/offshore flow is approximately balancing each other in the time mean, explaining the weak climatological mean winds (Fig. 1).

Together, the significance of diabatic heating and ageostrophic flow (Fig. 1), the evidence for diurnal wind reversals and ephemeral precipitation (Extended Data Fig. 1), and the stronger mid-Holocene monsoon circulation when mechanical stationary wave forcing was weaker and insolation higher (Fig. 2),

all refute the authors inference that the NAM is anything but a classic tropical monsoon circulation.

References

[1] Boos, W.R., Pascale, S.: Mechanical forcing of the North American monsoon by orography. Nature **599**(7886), 611–615 (2021). https://doi.org/10.1038/s41586-021-03978-2

[2] Broccoli, A.J., Manabe, S.: The effects of orography on midlatitude Northern Hemisphere dry climates. J Clim **5**(11), 1181–1201 (1992)

[3] Held, I.M.: Stationary and quasi-stationary eddies in the extratropical troposphere: Theory. Large-scale dynamical processes in the atmosphere **127**, 168 (1983)

[4] Held, I.M., Ting, M., Wang, H.: Northern winter stationary waves: Theory and modeling **16**, 2125–2144 (2002)

[5] Cerezo-Mota, R., Cavazos, T., Arritt, R., Torres-Alavez, A., Sieck, K., Nikulin, G., Moufouma-Okia, W., Salinas-Prieto, J.A.: CORDEX-NA: factors inducing dry/wet years on the North American Monsoon region. International Journal of Climatology **36**(2), 824–836 (2016)

[6] Pascale, S., Kapnick, S.B., Bordoni, S., Delworth, T.L.: The influence of CO2 forcing on North American monsoon moisture surges. Journal of Climate **31**(19), 7949–7968 (2018)

[7] Burk, S.D., Thompson, W.T.: The summertime low-level jet and marine boundary layer structure along the California coast. Monthly Weather Review **124**(4), 668–686 (1996)

[8] Doubler, D.L., Winkler, J.A., Bian, X., Walters, C.K., Zhong, S.: An NARR-Derived Climatology of Southerly and Northerly Low-Level Jets over North America and Coastal Environs. Journal of Applied Meteorology and Climatology **54**(7), 1596–1619 (2015)

[9] Boos, W.R., Korty, R.L.: Regional energy budget control of the intertropical convergence zone and application to mid-Holocene rainfall. Nature Geoscience **9**(12), 892–897 (2016)

[10] Brierley, C.M., Zhao, A., Harrison, S.P., Braconnot, P., Williams, C.J., Thornalley, D.J., Shi, X., Peterschmitt, J.-Y., Ohgaito, R., Kaufman, D.S., *et al.*: Large-scale features and evaluation of the PMIP4-CMIP6 midHolocene simulations. Climate of the Past **16**(5), 1847–1872 (2020)

[11] Metcalfe, S.E., Barron, J.A., Davies, S.J.: The Holocene history of the

North American Monsoon:'known knowns' and 'known unknowns' in understanding its spatial and temporal complexity. Quaternary Science Reviews **120**, 1–27 (2015)

[12] Bhattacharya, T., Tierney, J.E., Addison, J.A., Murray, J.W.: Ice-sheet modulation of deglacial north american monsoon intensification. Nature Geoscience **11**(11), 848–852 (2018)

[13] Fu, M., Cane, M.A., Molnar, P., Tziperman, E.: Warmer Pliocene Upwelling Site SST Leads to Wetter Subtropical Coastal Areas: A Positive Feedback on SST. Paleoceanography and Paleoclimatology **37**(2) (2022)

[14] Hersbach, H., Bell, B., Berrisford, P., Hirahara, S., Horányi, A., Muñoz-Sabater, J., Nicolas, J., Peubey, C., Radu, R., Schepers, D., *et al.*: The ERA5 global reanalysis. Quarterly Journal of the Royal Meteorological Society **146**(730), 1999–2049 (2020)
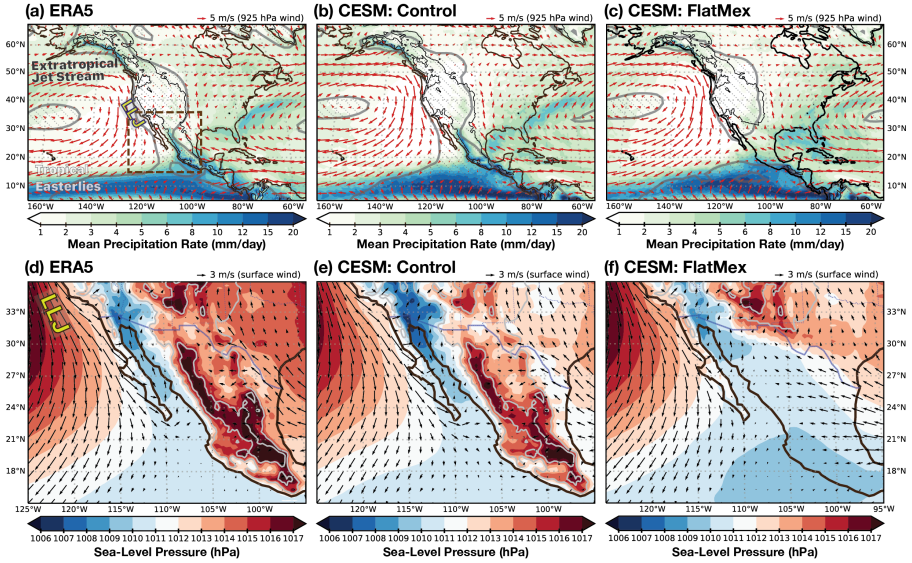
Fig. 1 Climatological circulation in reanalysis and model simulations: Panels (a)-(c) show July-September averages of precipitation (shading) and 925 hPa wind vectors (arrows) from the ERA5 [14] (1979-2021 CE), and the CESM control and *FlatMex* simulations from Ref. [1], respectively. Gray contours and faint diagonal hatching indicate regions where the ratio of the ∼950 hPa ageostrophic and geostrophic horizontal wind magnitude is of order unity or greater: $|\mathbf{v_a}|/|\mathbf{v_g}| \geq 1$ — the wind components were defined on the nominal 950 hPa CESM hybrid sigma-pressure level (third model level from the bottom) to match the continuous fields in ERA5. The geostrophic wind $|\mathbf{v_g}| = (u_g^2 + v_g^2)^{1/2}$ is the rotational part (i.e., derived from relative vorticity using *NCL* functions *uv2vrf* and *vr2uvf*) of the horizontal wind field $\mathbf{v} = (u, v)$, and the ageostrophic wind is defined as the residual $\mathbf{v_a} = \mathbf{v} - \mathbf{v_g}$. Bottom panels show the surface wind (arrays) and sea-level pressure (shading) in the region indicated by the black box in panel (a). Note the cross isobaric wind from the relative high sea-level pressure in the eastern North Pacific, over the Baja California peninsula and into the low-pressure region in Gulf of California and western Mexico. This circulation feature is also present north of ∼27°N in the *FlatMex* simulation (f), suggesting that it is primarily controlled by thermal rather than local orographic effects. Mapping software: Cartopy with Natural Earth shapefiles.
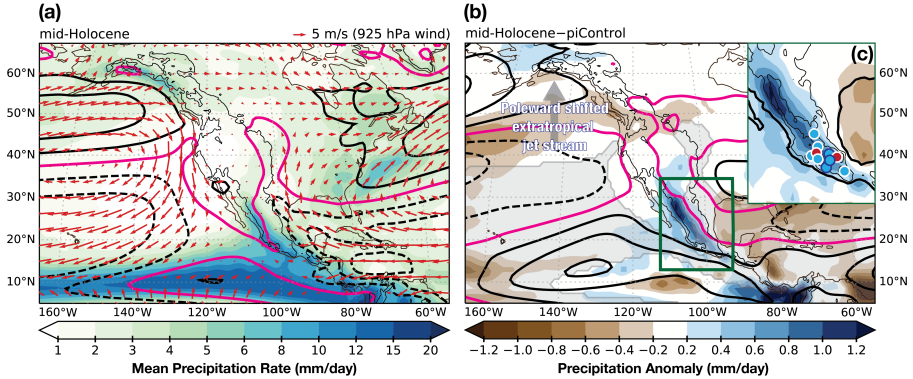
Fig. 2 Multi-model mean comparison of the mid-Holocene and pre-industrial control simulation from the fourth phase of the Paleoclimate Modelling Inter-comparison Project (PMIP4)[10]: (a) Climatological precipitation (shading), 925 hPa zonal wind (contours in 3 m/s increments), and wind vectors (arrows) from the mid-Holocene simulations. Westerly (easterly) zonal wind is indicated by solid (dashed) contours, and the red contours indicates the zero wind lines. (b) Precipitation anomaly (shading) and 925 hPa zonal wind anomaly (contours in 2 m/s increments) between the mid-Holocene and pre-industrial simulations. Gray shading indicates regions with negative zonal wind in the mid-Holocene climatology. (c) Precipitation anomaly (shading) with proxy-data evidence (circles) of changes in mid-Holocene NAM strength [11]. Blue (red) circles indicate increased (decreased) mid-Holocene NAM precipitation; multi (single) proxy evidence are indicated by a dark blue (white) border. Models were selected if both the mid-Holocene and pre-industrial simulations included a minimum of 100 years of monthly zonal and meridional wind and precipitation data. Multi-model climatologies are based: ACCESS-ESM1-5; AWI-ESM-1-1-LR; CESM2; EC-Earth3-LR; GISS-E2-1-G; INM-CM4-8; IPSL-CM6A-LR; MIROC-ES2L; MPI-ESM1-2-LR; and MRI-ESM2-0. Mapping software: Cartopy with Natural Earth shapefiles.
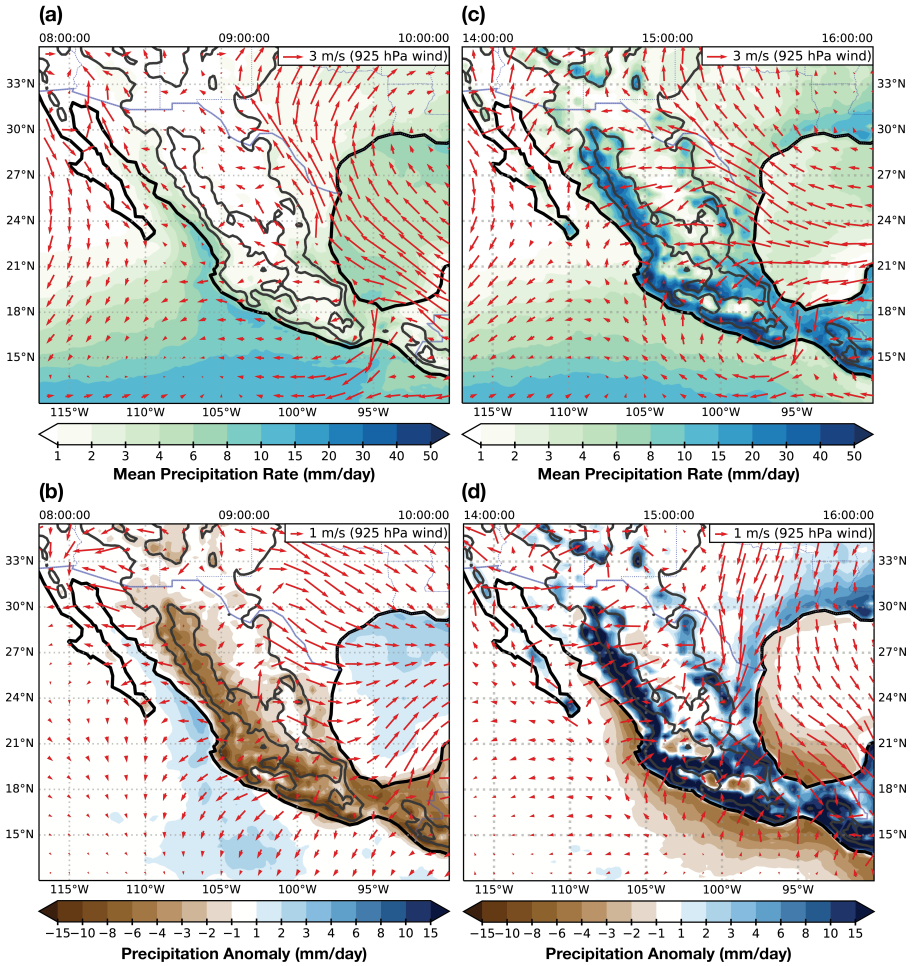
Extended Data Fig. 1 Diurnal cycle of 925 hPa winds and preciptiation in the ERA5 [14] reanalysis dataset: The top panels show climatological (1979-2021 CE) pre-cipitation (shading) and 925 hPa wind vectors (arrows) derived from 3-hourly instantaneous data for July-September (NAM season). The bottom panels show deviations from the daily mean. The left panels show the circulation in the morning at 09:00:00 local time (15:00:00 UTC) when the monsoon is weak, and the right panels the corresponding fields in the after-noon at 15:00:00 local time (21:00:00 UTC) when the monsoon is strong. Note that the wind is showing the quintessential fingerprint of a thermally driven monsoon, with an offshore (onshore) flow in the morning (afternoon) when the monsoon is weak (strong). This reversal of the flow is most clear in the anomaly fields in panels (b) and (d). 5 Mapping software: Cartopy with Natural Earth shapefiles.